Asymmetry, Nonlinearity, and Dynamics of El Niño Southern Oscillation

Nabil Swedan (nabilswedan@yahoo.com)
Pacific Engineering PLLC, Redmond, WA

Research Article

Keywords: El Niño, Oceanic Niño Index, Ocean, Atmosphere, Fluid hammer

Posted Date: February 15th, 2022

DOI: https://doi.org/10.21203/rs.3.rs-1322232/v1

Abstract

Asymmetry and nonlinearity of the observed Oceanic Niño Index (ONI) have been subjects of research for decades. The magnitude of the warming phase of the Index, or El Niño, is always greater than that of the succeeding cooling phase, or La Niña. In addition, the Index is damped with time. Such asymmetry and nonlinearity of ONI have remained un-captured by climate model simulations. Addressing these subjects satisfactorily is important for through comprehension of ENSO dynamics. This work proposes a potential explanation of the asymmetry and nonlinearity of ONI. El Niño Southern Oscillation is a product of an air hammer produced by atmospheric air forces in El Niño region. The resulting energy cycles between atmosphere and ocean are damped with time, just like pressure and energy cycles produced by water, steam, and air hammer experienced in practical applications. In analogy, the amplitude of the warming phase is greater than that of the succeeding cooling phase, and the Oceanic Niño Index exhibits nonlinearity with time. The physical explanation and theoretically derived Oceanic Niño Index agree with observations, and the theoretical index may therefore be used to assess ENSO climatology. This may have merit for research and society.

Introduction

Publication [1] provides a description of El Niño events, how and where they occur, their impact on the economy, as well as their imprint on world history. El Niño is a major event that can adversely affect the livelihoods of many regions of the world. Severe weather extremes including but not limited to heavy rainfall, strong winds, drought, and extreme temperatures are typically associated with El Niño. El Niño events occur towards the end of the year, during the southern hemispheric summer in the tropics west of South America. The related oscillation, El Niño Southern Oscillation (ENSO), is monitored by a number of El Niño indexes, some of which are described in [2, 3]. Generally, an index measures sea temperature fluctuation in a defined region in the tropics west of South America with respect to a base period of time. For the Oceanic Niño Index (ONI) considered for comparison with the work presented in this manuscript, El Niño region 3.4 is the defined region, located between (5°N-5°S, 120°W-170°W). It is located at the equator and observes nearly maximum temperature anomalies. National Oceanic and Atmospheric Administration [4] and National Center for Atmospheric Research [5] present calculation methodology and observed values of the Oceanic Niño Index. They are tabulated in Table 1 and plotted in Fig. 1 for the period of time between 1996 and 2020. Values of the Index within ±0.5°C are considered Niño neutral. Below this value, a cooling phase or episode typically referred to as Niña manifests. Values of the Index above ±0.5°C are referred to as Niño or warming phase or episode. This, however, is to be distinguished from El Niño event during which massive amount of energy is exchanged with the surroundings. The events are characterized by maximum amplitude of the Index. Figure 1, shows that two events occurred in the period of time in consideration, in 1996/1997 and 2014/2015. Also, the figure shows that the Index carried over in 1996 from the previous oscillation nearly -0.5°C. When this temperature anomaly is accounted for, Niño amplitudes are greater than those of La Niña. In addition, the amplitudes decrease with time.

Table 1
The observed Oceanic Niño index for Niño region 3.4, °C, obtained from the website of [4].

Year	DJF	JFM	FMA	MAM	AMJ	MJJ	JJA	JAS	ASO	SON	OND	NDJ	Annual average
1996	-0.90	-0.80	-0.60	-0.40	-0.30	-0.30	-0.30	-0.30	-0.40	-0.40	-0.40	-0.50	-0.47
1997	-0.50	-0.40	-0.10	0.30	0.80	1.20	1.60	1.90	2.10	2.30	2.40	2.40	1.17
1998	2.20	1.90	1.40	1.00	0.50	-0.10	-0.80	-1.10	-1.30	-1.40	-1.50	-1.60	-0.07
1999	-1.50	-1.30	-1.10	-1.00	-1.00	-1.00	-1.10	-1.10	-1.20	-1.30	-1.50	-1.70	-1.23
2000	-1.70	-1.40	-1.10	-0.80	-0.70	-0.60	-0.60	-0.50	-0.50	-0.60	-0.70	-0.70	-0.83
2001	-0.70	-0.50	-0.40	-0.30	-0.30	-0.10	-0.10	-0.10	-0.20	-0.30	-0.30	-0.30	-0.30
2002	-0.10	0.00	0.10	0.20	0.40	0.70	0.80	0.90	1.00	1.20	1.30	1.10	0.63
2003	0.90	0.60	0.40	0.00	-0.30	-0.20	0.10	0.20	0.30	0.30	0.40	0.40	0.26
2004	0.40	0.30	0.20	0.20	0.20	0.30	0.50	0.60	0.70	0.70	0.70	0.70	0.46
2005	0.60	0.60	0.40	0.40	0.30	0.10	-0.10	-0.10	-0.10	-0.30	-0.60	-0.80	0.03
2006	-0.90	-0.80	-0.60	-0.40	-0.10	0.00	0.10	0.30	0.50	0.80	0.90	0.90	0.06
2007	0.70	0.20	-0.10	-0.30	-0.40	-0.50	-0.60	-0.80	-1.10	-1.30	-1.50	-1.60	-0.61
2008	-1.60	-1.50	-1.30	-1.00	-0.80	-0.60	-0.40	-0.20	-0.20	-0.40	-0.60	-0.70	-0.78
2009	-0.80	-0.80	-0.60	-0.30	0.00	0.30	0.50	0.60	0.70	1.00	1.40	1.60	0.30
2010	1.50	1.20	0.80	0.40	-0.20	-0.70	-0.10	-1.30	-1.60	-1.60	-1.60	-1.60	-0.40
2011	-1.40	-1.20	-0.90	-0.70	-0.60	-0.40	-0.50	-0.60	-0.80	-1.00	-1.10	-1.00	-0.85
2012	-0.90	-0.70	-0.60	-0.50	-0.30	0.00	0.20	0.40	0.40	0.30	0.10	-0.20	-0.15
2013	-0.40	-0.40	-0.30	-0.30	-0.40	-0.40	-0.40	-0.30	-0.30	-0.20	-0.20	-0.30	-0.33
2014	-0.40	-0.50	-0.30	0.00	0.20	0.20	0.00	0.10	0.20	0.50	0.60	0.70	0.11
2015	0.50	0.50	0.50	0.70	0.90	1.20	1.50	1.90	2.20	2.40	2.60	2.60	1.46
2016	2.50	2.10	1.60	0.90	0.40	-0.10	-0.40	-0.50	-0.60	-0.70	-0.70	-0.60	0.33
2017	-0.30	-0.20	0.10	0.20	0.30	0.30	0.10	-0.10	-0.40	-0.70	-0.80	-1.00	-0.21
2018	-0.90	-0.90	-0.70	-0.50	-0.20	0.00	0.10	0.20	0.50	0.80	0.90	0.80	0.01
2019	0.70	0.70	0.70	0.70	0.50	0.50	0.30	0.10	0.20	0.30	0.50	0.50	0.48
2020	0.50	0.50	0.40	0.20	-0.10	-0.30	-0.40	-0.60	-0.90	-1.20	-1.30	-1.20	-0.37

References [6, 7] present overviews of the scientific evolution of ENSO understanding, ENSO mechanisms, and the related hypotheses and theories, and provide a large number of references for further reading on the subject. Although ENSO has become increasingly known to the scientific community, more research in this field is recommended by these overviews. Self-sustained oscillators that work together to alter thermocline depth anomalies and maintain ENSO steady. The oscillators are products of ocean-atmosphere interactions with negative feedbacks from ocean and atmosphere that sustain the oscillation indefinitely. An and Jin [8] reveal that this ENSO scientific understanding does not explain the

nonlinear nature of ENSO. Although climate models simulate sea temperature anomalies well, they do not appear to capture the observed asymmetry in sea temperature anomalies, [9]. These are fundamental requirement for a complete understanding of El Niño Southern Oscillation.

This work suggests that because ENSO amplitude decreases with time, it requires continual energy supply. The energy is provided by air hammers that occur during El Niño events. When air flow decreases significantly during the events, atmospheric air forces produce energy cycles, similar to the energy cycles observed in practical air hammer applications. Energy cycles develop between ocean and atmosphere in El Niño region that are damped with time, Fig. 2. They are asymmetric and nonlinear as observed. To explain these features of ENSO, the equation of the Oceanic Niño Index is derived and validated based on data and observations available, it is an involved mathematical exercise. For simplicity, a section entitled “Symbols and abbreviations” is provided. The intended meanings of symbols used to derive the theoretical equation of the Index are explained in this section.

Background Information

As per the discussion in Introduction and Fig. 1, ENSO is a damped oscillation. However, because the period of time between two consecutive El Niño events has decreased [10], ENSO appears to be a continuous oscillation. To maintain the oscillation, there has to be energy supply, and there are no sources of energy in ocean surface or atmosphere.

El Niño event is a major thermodynamic process and requires a massive amount of heat and sufficient sea temperature rise for its evolution based on the current state of thermodynamic understanding [11]. The sun provides this heat in the form of warm water because poleward heat transport has decreased [12]. Less solar heat is conveyed poleward, and solar heat anomaly in the form of warm water is thus produced in the hydrosphere. Because global rise in average temperature is least in the tropics, average sea level expansion is least in the tropics as well. The tropics have, therefore, become low locations, and the warm water gradually accumulates in the tropics with time. It appears that when heat accumulation is large enough, tropical Pacific winds are weakened considerably [13]. Simultaneously, the warm water heads east steadily like a slick of oil as [1] describes the process. The warm water provides heat supply to El Niño throughout the entire duration of the event. In the data section and Table 2, the solar heat of El Niño is calculated to be nearly equal to 5.65×10^{21} J; it is of the same order of magnitude of all of the energy of seasonal typhoons combined. The sample calculations show that the upward air flow rate in El Niño region reduces from $M=1.45 \times 10^{11}$ kg s^{-1} to $M_n=3.09 \times 10^{9}$ kg s^{-1} during El Niño. Air flow decreases by nearly 98.0%; it is virtually arrested and air hammer occurs and energy cycles develop between ocean and atmosphere in the region as a result.

Table 2

Calculation of solar heat of El Niño, Q_{sn}, between El Niño event of 1996/197 and that of 2014/2015. The symbol NH is the abbreviation for northern hemisphere and SH is the abbreviation for southern hemisphere. T_{SHi}-T_{NHi} is the observed difference in annual average sea temperature between the hemispheres. The observed anomalies of annual average sea temperatures for an arbitrary year, i, are obtained from [17].

Year	Anomalies of annual average sea temperature NH, ˚C	Anomalies of annual average sea temperature SH, ˚C	T_{SHi}-T_{NHi} ˚C	Cumulative solar heat Q_{sn}, J
1997	0.322	0.281	-0.04	0.00E+00
1998	0.413	0.394	-0.019	4.98E+19
1999	0.212	0.213	0.001	4.72E+19
2000	0.244	0.204	-0.040	1.52E+20
2001	0.340	0.327	-0.013	1.86E+20
2002	0.363	0.350	-0.013	2.20E+20
2003	0.449	0.323	-0.126	5.52E+20
2004	0.467	0.243	-0.224	1.14E+21
2005	0.484	0.303	-0.181	1.62E+21
2006	0.440	0.290	-0.150	2.01E+21
2007	0.386	0.224	-0.162	2.44E+21
2008	0.352	0.190	-0.162	2.87E+21
2009	0.417	0.361	-0.056	3.01E+21
2010	0.456	0.362	-0.094	3.26E+21
2011	0.317	0.278	-0.039	3.36E+21
2012	0.413	0.287	-0.126	3.69E+21
2013	0.451	0.303	-0.148	4.08E+21
2014	0.617	0.335	-0.282	4.83E+21
2015	0.737	0.425	-0.312	5.65E+21

Fluid hammer is a known phenomenon in practical applications. It is experienced daily when a valve on a domestic water line is shut suddenly. In industry, steam and air hammers occur as well when fluid flow is reduced significantly in a short period of time. The phenomenon is well addressed in the literature and typical textbooks or references of fluid dynamics, for example [14]. It is a localized and transient phenomenon, restricted to fluid streams subjected to a sudden and major flow reduction. Energy cycles in the form of fluid pressure develop that are damped with time. In analogy, ENSO energy cycles appear to develop following significant air flow reduction during El Niño events. They are localized in El Niño region, and energy is exchanged between atmosphere and sea water in the region. If the potential energy of the atmosphere increases, sea temperature decreases and vice versa, which is observed [15]. The authors observed an inverse relationship between height of tropical tropopause and sea temperature in El Niño region, thus suggesting the existence of potential energy cycles of the air mass, a characteristic property of an air hammer. Sea temperature should, therefore, exhibit damped fluctuations with time, which is observed as well as discussed in Introduction. Base on this

understanding, the governing equation of the oscillation is derived and sample calculations are provided, typical for the entire period of time in consideration between 1996 and 2020. They are presented in Table 3 and Fig. 2 for discussion and conclusions.

Table 3. Calculation of the Oceanic Nino Index for the period of time between 1997 and 2020

year	1997	1998	1999	2000	2001	2002	2003	2004
Year count from 2016	1	2	3	4	5	6	7	8
Phase angle, degrees	70.37	140.74	211.11	281.48	351.85	422.23	492.60	562.97
$Z(t)/Z_{min}$	0.852	0.52	-0.38	-0.66	-0.09	0.48	0.36	-0.18
Surface heat, $Q_s(t)$, J	4.8E+21	2.5E+21	-1.8E+21	-3.2E+21	-4.1E+20	2.3E+21	1.9E+21	-8.4E+20
Oceanic Nino Index, °C	2.10	1.09	-0.80	-1.38	-0.18	1.02	0.76	-0.37

Table 3-continues

Year	2005	2006	2007	2008	2009	2010	2011	2012
Year count from 2016	9	10	11	12	13	14	15	16
Phase angle, degrees	633.34	703.71	774.08	844.45	914.82	985.19	1055.56	1125.94
$Z(t)/Z_{min}$	-0.40	-0.10	0.27	0.25	-0.07	-0.24	-0.09	0.14
Surface heat, Qs(t), J	-1.9E+21	-4.9E+20	1.3E+21	1.2E+21	-3.4E+20	-1.2E+21	-4.4E+20	6.9E+20
Oceanic Nino Index, °C	-0.85	-0.21	0.56	0.52	-0.15	-0.51	-0.19	0.30

Table 3-continues

Year	2013	2014	2015	2016	2017	2018	2019	2020
Year count from 2016	17	18	19	20	21	22	23	24
Phase angle, degrees	1196.31	1266.68	1337.05	1407.42	1477.79	1548.16	1618.53	1688.90
$Z(t)/Z_{min}$	0.16	-0.02	0.85	-0.44	0.46	0.64	0.01	-0.51
Surface heat, Qs(t), J	7.8E+20	-9.4E+19	4.7E+21	-2.1E+21	2.2E+21	3.0E+21	6.3E+19	-2.4E+21
Oceanic Nino Index, °C	0.34	-0.04	2.19	-0.77	1.07	1.44	0.16	-0.92

Data And Method

The objective of this work is to derive the mathematical equation governing the Oceanic Niño Index and compare Index calculated values with observed ones. For this endeavor, the physical parameters of ocean and atmosphere prior and during an El Niño event should be defined. These parameters dictate equation terms. Important physical parameters are

solar heat of El Niño, area and location of El Niño event, air flow rate prior and during the event, sea temperature at which the event occurs, and structure of the ocean and atmosphere. Publication [3] discusses spatial and temporal evolution of El Niño. As Fig. 13 of this reference and its related discussion indicate, statistically significant El Niño warming may be assumed to cover nearly 70% to 80% of the surface area between the tropics (±23.4°) and 70°W to 180°E. Therefore, El Niño region has surface area that is nearly equal to A_n=4.91 x 10^{13} m^2.

The value of solar heat of El Niño, Q_{sn}, is required, and it may be estimated by knowing the maximum sea surface temperature anomaly, which is nearly equal to 2.5 °C, measured at Niño region 3.4. Because surface winds are virtually arrested, sea water temperature rise in the ocean mixed layer of the region, the top 95 meters, is not uniformly mixed. Warm water stratifies and accurate temperature profile is unavailable. The temperature profile is likely to decrease logarithmically with depth measured from ocean surface. Assuming linearity for simplicity, the center of mass of the triangle enclosed by the temperature profile and ocean depth is located at one third of the depth measured from surface water. Therefore, Q_{sn} would be nearly equal to the thermal capacity of the top 95 meters multiplied by one-third of average sea surface temperature rise. Because this rise is nearly equal to one-half of the maximum sea surface temperature rise, Q_{sn} is nearly equal to the thermal capacity of the top 95 meters multiplied by one-sixth of the maximum sea surface temperature rise of 2.5 °C. Therefore, $Q_{sn} \approx A_n\ d_m\ \delta_{sw}\ Cp_{sw}$ x (2.5/6), where A_n is area of El Niño region, 4.91 x 10^{13} m^2; d_m is average depth of the ocean mixed layer, 95 m; δ_{sw} is density of sea water, 1 048 kg m^{-3}; and Cp_{sw} is specific heat of sea water, 3 980 J kg^{-1} $°C^{-1}$. The value of Q_{sn} should thus be slightly less than 8.11 x 10^{21} J.

Alternatively, the solar heat of El Niño, Q_{sn}, may be calculated by considering variation in poleward heat transport between two consecutive El Niño events. The poleward heat transport is solar heat in the form of warm water flux, and its variation produces solar heat anomaly in the hydrosphere. There exists a correlation between the difference in sea temperature between the hemispheres and the solar heat anomaly [12]. At the seasonal level, the difference alters seasonal values of poleward heat transport; it fluctuates between a minimum of 12% and a maximum of 134% with respect to its average value, which is observed [16]. Such a large fluctuation in poleward heat transport provides seasonal solar energy of tropical cyclones. The estimated seasonal energy of typhoons is nearly 9.38 x 10^{21} J. Similarly, the northern hemisphere has been warming more than the southern hemisphere as the data source of Table 2 shows. This uneven warming trend between the hemispheres has decreased the poleward heat transport by nearly 1.2%, and the solar heat may be calculated. Derivation of the following equation that may be used to calculate Q_{sn} is discussed in detail by [12], which may be summarized for, n, years as follows:

$$Q_{sn}=\sum_{i=1}^{n}-[\{(0.2+\beta\ d_m \times (T_{SHi}-T_{NHi}))/0.2\}^{0.5}-1] \times PHT$$

Where

Q_{sn}=Cumulative solar heat of El Niño in, n, years, J.

n =Number of years between two consecutive El Niño events, yr.

β =Sea water volumetric thermal expansion, 200 x 10^{-6} $°C^{-1}$.

d_m =Average depth of the ocean mixed layers, 95 m.

T_{SHi}=Sea temperature of the southern hemisphere for an arbitrary year, i, °C.

T_{NHi}=Sea temperature of the northern hemisphere for an arbitrary year, i, °C.

PHT=Poleward heat transport, 5.52 x 10^{22} J yr^{-1}.

The negative sign upfront of the square brackets is a convention to indicate that variation in the solar heat is a decrease in the heat budget of the northern hemisphere. Regardless of which hemisphere warms more, there would be a positive Q_{sn} that ultimately accumulates in the tropics. The values of T_{SHi} and T_{NHi} are available in the literature, for example [17]. This reference provides marine temperature anomalies for the southern and northern hemispheres. They are tabulated in Table 2 for the period of time between the two El Niño events of 1996/1997 and 2014/2015. The solar heat Q_{sn} is calculated as warm water as follows: For 1998, the observed T_{SHi}-T_{NHi}=-0.019 °C, and the solar heat is equal to -[{(0.2+200 x 10^{-6} x 95 x -0.019)/0.2}$^{0.5}$-1] x 5.52 x 10^{22}=4.98 x 10^{19} J. For 1999, T_{SHi}-T_{NHi}=0.001°C, and the cumulative solar heat is equal to -[{(0.2+200 x 10^{-6} x 95 x 0.001)/0.2}$^{0.5}$-1] x 5.52 x 10^{22}+4.98 x 10^{19}=4.72 x 10^{19} J. The calculations are repeated through 2015, and the cumulative value of Q_{sn} is equal to 5.65 x 10^{21} J. It is slightly less than 8.11 x 10^{21} J calculated earlier as expected. The advantage of calculating solar heat Q_{sn} using temperature difference between the hemispheres is that heat value may be projected with time by knowing temperature trends. The heat increases sea temperature in El Niño region, and when the temperature approaches 28 °C, El Niño event occurs based on [4].

For the objectives of this manuscript, the relevant atmospheric air and ocean dynamical parameters in El Niño region are schematically illustrated in Fig. 3. Before and after an El Niño event, Fig. (3a), tropical winds have horizontal, v_h, and vertical, v, velocity components. The vertical air mass flow rate M is at steady state as dictated by astronomical parameters. This fraction of the total tropical air circulation exchanges heat between sea water and tropical tropopause. Its value is nearly equal to 1.45 x 10^{11} kg s^{-1}, calculated in the Sample calculations. The air flow M removes heat from surface water as latent heat of water evaporation. At tropical tropopause having height Z_T, water vapor condenses completely. The air flow M then returns to the surface to remove surface heat again, and the cycle repeats. The textbook [18] presents the U.S. standard atmosphere. At tropopause, nearly 20 kPa, the global average height of tropopause Z_T is 1.2 x 10^4 m. For the tropics at 28 °C, Z_T is thus approximately equal to 1.25 x 10^4 m. Global average air density, δ, at 50 kpa is approximately equal to 0.736 kg m^{-3}. Therefore, average air density in the tropics, δ_n, is nearly 0.704 kg m^{-3}. The solar heat of El Niño, $Q_{sn,}$ on the other hand may be thought of as solar heat denied to the northern hemisphere, it is thus shown as warm water transferred from the northern hydrosphere to the southern hydrosphere. Because of the large amount of heat accumulation during El Niño, the flow rate of tropical winds decreases following a transient and potentially random process whose final scenario may be schematically illustrated by Figure (3b). The horizontal component of tropical winds is negligible and the flow rate, M, decreases from 1.45 x 10^{11} kg s^{-1} to M_n of 3.09 x 10^9 kg s^{-1} as shown in the calculation section. Air flow rate reduces by nearly 98% in a short period of time. Such a reduction produces an air hammer and energy cycles develop. These cycles have no net energy exchanged with the surroundings, only in El Niño region between sea water and atmosphere, where the air hammer occurs. If the atmosphere gains potential energy, the surface loses an equal amount of energy and vice versa. The solar heat, Q_{sn}, is gradually removed from sea water and returned to the northern hemisphere by global air circulation. Because the event involves removal of climate system internal heat by evaporating water, the air column between sea level and tropopause is assumed to be engaged in El Niño thermodynamic evolution. Accordingly, the theoretical mathematical equation of Oceanic Niño Index is derived.

Required for application of the derived equations are values of evaporation and water vapor mixing ratio at saturation in El Niño region. The report [19] estimated average global precipitation to be about 2.61±0.23 mm day^{-1}, which is equal to global evaporation. However, at the regional level evaporation is not necessarily equal to precipitation. In the tropics, evaporation must be greater than precipitation, for much of tropical moisture travels to higher latitudes.

Meteorological records and evaporation data do not appear to be available for El Niño region at this time. A comprehensive analysis of evaporation study in Peru using a piche evaporimeter was prepared by [20]. The results are summarized in table 2 of this reference. For weather stations having elevation near sea level and highest temperatures, 22 °C or more (stations 1, 2, 11, and 12), average annual evaporation is 4.93 mm d^{-1} at average temperature of 22.78 °C. Application of equation 21 of [21] at average temperature of 22.78 °C gives average annual evaporation of 4.3 mm d^{-1}. Because annual average sea temperature in El Niño region is greater than 22.78 °C, nearly 28 °C, the equation gives 6.08 mm d^{-1} for evaporation. The psychometric chart [22] gives 0.0238 kg water per kg dry air for water vapor mixing ratio at saturation temperature of 28 °C.

THEORY AND ANALYSIS

In this section, dynamics of the air mass in El Niño region before and during an El Niño event is analyzed based on the present understanding of atmospheric physics. Referring to Fig. (3b), the horizontal velocity of surface winds, v_h, is nearly arrested during El Niño, and, therefore, the vertical components of atmospheric air flow and forces are relevant for the objectives of this work. Before El Niño, Fig. (3a), the upward air mass flow rate, M, is assumed to be at a steady state having vertical velocity v. Air flow and velocity decrease substantially during El Niño to M_n and v_n respectively, Fig. (3b). The textbooks [18, 23] discuss atmospheric air related properties, physics, thermodynamics, forces, and equations of motion. For the volume of air in consideration that is enclosed by the dashed lines of figures (3a) and (3b), the resultant of atmospheric force may include buoyant upward force, Coriolis force, and variation in air mass momentum flux through volume boundary. Before an El Niño event, the component of the resultant of atmospheric force in Z direction, or vertical to the surface, may be written as follows:

$$F_z=F_b+F_{cz}+d(m\ v)/dt \qquad (1)$$

Where

F_z=Component of the resultant of atmospheric force in Z direction, N.

F_b=Buoyant upward force, N.

F_{cz}=Component of Coriolis force in Z direction, N.

$d(m\ v)/dt$=Variation in the flux of air mass momentum through volume boundary, N.

m =Mass of air in the volume in consideration of El Niño region between sea level and tropical tropopause, kg.

v =Air velocity, m s^{-1}.

t =Time, s.

In Eq. (1), friction forces in Z direction are not considered because air streams move upward, away from the surface, and velocity gradients between the air streams may be neglected. Although the warm mass of air in El Niño region is large and straddles the equator, it is only 4% or less of the total mass of the surrounding colder atmospheric air. The force of buoyancy may be expressed as follows:

$$F_b=(\delta-\delta_n)\ A_n\ Z_T\ g \qquad (2)$$

Where

δ =Average density of the surrounding air, 0.736 kg m^{-3}.

δ_n =Average air density in El Niño region, 0.704 kg m^{-3}.

A_n =Area of El Niño region, 4.91 x 10^{13} m^2.

Z_T =Height of tropical tropopause, 1.25 x 10^4 m.

g =Gravity acceleration, 9.8 m s^{-2}.

The component of Coriolis force in Z direction, F_{cz}, may be obtained from the total force of Coriolis

$\mathbf{F_c} = -2\ m\ \boldsymbol{\omega} \times \mathbf{v_r} - 2\ m\ \boldsymbol{\omega} \times d\mathbf{Z(t)}/dt$ (3)

Where

$\mathbf{F_c}$=Total force of Coriolis, N.

$\boldsymbol{\omega}$=Angular velocity of the earth around its axis, 7.27 x 10^{-5} radians s^{-1}.

$\mathbf{v_r}$=Relative velocity between the air mass in El Niño region and surface, m s^{-1}.

$d\mathbf{Z(t)}/dt$=Variation in the height of the air mass in El Niño region with time, m s^{-1}.

The symbols in bold font of Eq. (3) indicate vectors and their cross products. During El Niño, there is no tangible horizontal movement of the mass of air m. Therefore, air mass relative velocity with respect to the surface, $\mathbf{v_r}$, may be neglected. The first term on the right hand side of Eq. (3), -2 m $\boldsymbol{\omega}$ x $\mathbf{v_r}$, may thus be discarded. The second term of the equation, -2 m $\boldsymbol{\omega}$ x $d\mathbf{Z(t)}/dt$, is always perpendicular to Z and can have no component in Z direction. The term F_{cz} of Eq. (1) may be omitted as well.

The last term of Eq. (1), d(m v)/dt, is required because the boundary of the volume of air in consideration, the dashed lines of Fig. (3), which encloses the air mass, m, is permeable. As this mass of air, m, rises upward under the force, F_b, some of the surrounding colder and denser air infiltrates into the air volume. As air mass is exchanged through volume boundary, variation in the flux of air mass momentum occurs. The variation must be equal to d(m v)/dt. At steady state before El Niño event, the net atmospheric force and its components are nearly equal to zero. Therefore, Fz≈0 and v is about constant, and the term d(m v)/dt of Eq. (1) simplifies

$d(m\ v)/dt = v\ dm/dt + m\ dv/dt = v\ dm/dt$ (4)

The term (m dv/dt) of Eq. (4) is equal to zero because the velocity v is constant. At steady state and for F_{cz}≈0, equations 1, 2, and 4 give

$0 = (\delta - \delta_n)\ A_n\ Z_T\ g + v\ dm/dt$ (5)

At steady state during El Niño event and for F_{cz}≈0, equations 1, 2, and 4 give

$0 = (\delta - \delta_n)\ A_n\ Z_{Tn}\ g + v_n\ dm/dt$ (6)

Where

Z_{Tn} =Height of tropical tropopause during El Niño event, m.

v_n =Vertical air velocity during El Niño event, m s^{-1}.

The right hand sides of equations (5) and (6) are similar to the right hand side of Eq. (1). The difference between them is equal to variation in atmospheric force, F_{zn}, when air flow decelerates from M to M_n. Therefore

$$-dF_{zn} =(\delta-\delta_n)\, A_n\, Z_{Tn}\, g + v_n\, dm/dt-(\delta-\delta_n)\, A_n\, Z_T\, g-v\, dm/dt \qquad (7)$$

Where

$-F_{zn}$ =Component of atmospheric force in Z direction during El Niño event, N.

The term dF_{zn} on the left hand side of Eq. (7) is equal to $d(m\, d^2Z/dt^2)=(dm/dt)\, d^2Z/dt^2 \times dt+m\, d^3Z/dt^3 \times dt$. If air deceleration, d^2Z/dt^2, is assumed to be about constant with time, then $d^3Z/dt^3\approx0$ and $dF_{zn}\approx(dm/dt)\, d^2Z/dt^2\, dt$. The term (dm/dt) of this equation represents variation, or increase, in air mass above El Niño region that is required to remove El Niño heat from sea water. It is equal to the air mass flow rate M_n as required by air mass balance. Therefore, $dF_{zn}\approx M_n\, d^2Z/dt^2\, dt$. If the period of time, dt, is selected to be equal to one complete cycle, or one year as will be discussed later in this section, then Eq. (7) yields the following relationship:

$$-M_n\, d^2Z(t)/dt^2=(\delta-\delta_n)\, A_n\, (Z_{Tn}-Z_T)\, g + dm/dt\, (v_n-v) \qquad (8)$$

Where

M_n =Annual air mass flow rate during El Niño, 3.09×10^9 kg s^{-1}.

The difference, $(Z_{Tn}-Z_T)$, represents variation in the height, Z(t), of the tropopause or air mass above sea water in El Niño region. The difference (v_n-v) is equal to dZ(t)/dt. Therefore, Eq. (8) gives

$$M_n\, d^2Z(t)/dt^2+(dm/dt)\, dZ(t)/dt+(\delta-\delta_n)\, A_n\, g\, Z(t)=0 \qquad (9)$$

Where

Z(t)=Variation in height of tropical tropopause or air mass above sea water in El Niño region, m.

Equation (9) is a differential equation of the second order. Its solution contains two arbitrary constants at initial conditions; specifically, initial phase angle and initial amplitude. These conditions may be obtained from the observed Oceanic Niño Index. For comparison with the observed Oceanic Niño Index of Fig. 1, the initial phase angle may be assumed to be equal to zero at time t=0. The annual average value of the Index, the red plot of Fig. 1, shows that nearly one year (1997 to 1998 and 2015 to 2016) is required to remove the solar heat. This may not be a coincidence: Just like seasonal variation, El Niño events appear to require one year to remove the entire solar heat from sea water. Thermodynamics of the earth is a repeatable process every year. Seasonal variation and El Niño are thermodynamic transformations differentially displaced from equilibrium. Based on the present state of thermodynamic understanding [11], they may be considered as reversible transformations. Therefore, the sum of variation in surface heat and variation in energy of the atmosphere is equal to zero at the completion of a full revolution of the earth around the sun. This is a thermodynamic requirement of the earth system dictated by astronomical parameters, which agrees with basic observations. Consequently, the time required for El Niño event to complete one cycle may be assumed to be equal to one year. Based on this discussion and Fig. 1, at time t=1 yr, phase angle is equal to 90°, and $Z(t)=Z_{min}$ and

$$Z(t)= Z_{min}\, Exp[-(dm/dt)\, t/2M_n] \times \sin [t\{(\delta-\delta_n)\, A_n\, g/M_n-\{(dm/dt)/2M_n\}^2\}^{0.5}] \qquad (10)$$

$$Z(t)/Z_{min}= Exp[-(dm/dt)\, t/2M_n] \times \sin [t\{(\delta-\delta_n)\, A_n\, g/M_n-\{(dm/dt)/2M_n\}^2\}^{0.5}] \qquad (11)$$

Where

Z_{min} =Initial amplitude of ENSO oscillation, m

Z(t) =Instantaneous amplitude of ENSO oscillation, m

On the other hand, variation in the height of an air mass Z(t) and variation in surface heat are correlated. When an air mass having unit mass gains heat, dQ_a, from the surface, air internal energy and potential energy increase in accordance with the first law of thermodynamics [11]:

$$dQ_a=dU+dW \quad (12)$$

$$-dQ_s=dQ_a \quad (13)$$

Where

dQ_a=Heat gained by unit air mass, J kg^{-1}.

dU=Internal energy gained by unit air mass, J kg^{-1}.

dW=Work produced by unit air mass, J kg^{-1}.

dQ_s=Heat lost by the surface per unit air mass, J kg^{-1}.

$$-dQ_s= dQ_a=dU+g\, dZ(t)/2 \quad (14)$$

The division of dZ(t) by 2 in Eq. (14) is required because the potential energy must be calculated at average variation in the height of the air mass. Because heat exchange between surface and atmosphere occurs slowly with time, equilibrium may be assumed and $dU \approx g\, dZ(t)/2$. Also, this conclusion is in line with the law of equipartition of energy. Therefore, Eq. (14) gives $-dQ_s=2\, g\, dZ(t)/2=g\, dZ(t)$. Or, variation in the potential energy of atmospheric air mass is equal to the opposite sign of variation in surface heat. This correlation may be used to convert fluctuation in the height of the air mass Z(t) of Eq. (10) into variation in surface heat as follows:

$$Q_s(t)=Q_{sn} \times Z(t)/Z_{min} \quad (15)$$

Where

$Q_s(t)$=Instantaneous variation in heat content of sea water in El Niño region, J.

The fluctuations of the instantaneous heat, $Q_s(t)$, produces ENSO warming and cooling episodes in El Niño region, damped with time, long after the entire heat Q_{sn} has been removed from sea water. To calculate surface temperature variation of these episodes, the following heat and mass balance may be used based on the discussion in the method section:

$$\Delta T_{sn} =Q_s(t)/[M\, C_p] \quad (16)$$

$$E =M\, (W_s-W_t) \quad (17)$$

Where

T_{sn} =Average sea surface temperature in El Niño region, °C.

ΔT_{sn} =Variation in average sea surface temperature of El Niño region, which is equal to variation in sea surface air temperature in the region, °C.

C_p =Air specific heat, 1 000 J kg^{-1} $°C^{-1}$.

E =Annual average evaporation in El Niño region, 1.09 x 10^{17} kg yr^{-1}.

M =Annual average air flow rate in El Niño region, 4.58 x 10^{18} kg yr^{-1}.

W_s =Average water vapor mixing ratio at saturation in tropics, 0.0238 kg water per kg dry air, dimensionless.

W_t =Water vapor mixing ratio at tropopause, 0.0 kg water per kg dry air, dimensionless.

ΔT_{sn} is equal to average sea surface temperature anomaly of the entire El Niño region. At the equator where Niño region 3.4 is defined, sea surface temperature observes maximum variation, which may be assumed to be equal to two times ΔT_{sn}. The temperature anomaly in Niño region 3.4 is by definition equal to the Oceanic Niño Index. By eliminating M from equations (16) and (17), the Index may be presented as follows:

$$\text{Oceanic Niño Index (ONI)} = 2 \times Q_{sn} \times [Z(t)/Z_{min}] \times W_s/(E\ C_p) \quad (18)$$

SAMPLE CALCULATIONS AND ERROR ESTIMATION

Accurate solution of the derived equations for short periods of time and accounting for seasonal variability of poleward heat transport, eleven-year solar cycle, and global temperature rise may be the ideal methodology. Calculations on annual basis may provide useful information of El Niño Southern oscillation as well. The advantage of conducting calculations on an annual basis is that seasonal variability of the poleward heat transport is eliminated. Required for application of Eq. (18) is the value of dm/dt, which is part of the decay factor of the oscillation $(dm/dt)/2M_n$. The value of dm/dt is a constant, dictated by astronomical parameters and represents variation in the mass of atmospheric air for any given latitude in one year. If the mass of air is imagined to have a uniform temperature and density, δ, or enclosed by an impermeable stack membrane at every latitude, then dm/dt=0 for every latitude. However, lower latitudes are warmer and more buoyant than the surrounding higher latitudes, and air mass infiltration from the surroundings is expected. Therefore, dm/dt≠0, and the value of dm/dt may be estimated for all latitudes in general and El Niño region in particular as follows:

$$dm/dt \approx \Delta m/\Delta t = (\delta V - \delta_n V)/t \quad (19)$$

$$dm/dt \approx [(\delta - \delta_n)\ A_n\ Z_T]/\tau \quad (20)$$

Where

V=Volume of the air mass above sea water in El Niño region, m^3.

τ=Time of one revolution of the earth around the sun, 3.15 x 10^7 s.

Example:

Evaporation caused by El Niño heat, $E_n=Q_{sn}$/Latent heat of water evaporation, $E_n=Q_{sn}/2.44 \times 10^6=5.65 \times 10^{21}/2.44 \times 10^6=2.32 \times 10^{15}$ kg yr^{-1}.

Air flow rate during El Niño, $M_n=E_n/W_s=2.32 \times 10^{15}/(0.0238 \times 3.15 \times 10^7)=3.09 \times 10^9$ kg s^{-1}, Eq. (17).

$dm/dt=(\delta-\delta_n)\ A_n\ Z_T/3.15 \times 10^7=(0.736-0.704) \times 4.91 \times 10^{13} \times 1.25 \times 10^4\ /3.15 \times 10^7=6.23 \times 10^8$ kg s^{-1}, Eq. (20).

Argument terms of the sinusoidal function:

$(\delta-\delta_n)\ A_n\ g/M_n=(0.736-0.704) \times 4.91 \times 10^{13} \times 9.8/\ 3.09 \times 10^9=4983.10$.

$\{(dm/dt)/2M_n\}^2=\{(6.23 \times 10^8)/2 \times 3.09 \times 10^9\}^2=0.01$.

For 1997, t=1 yr.

Oscillation decay factor $(dm/dt) \times t/2M_n=(6.23 \times 10^8) \times 1/(2 \times 3.09 \times 10^9)=0.10$.

Phase angle$=[t \times \{(\delta-\delta_n)\ A_n\ g/M_n-\{(dm/dt)/2M_n\}^2\}^{0.5}]=[1 \times \{4983.1-0.01\}^{0.5}]=70.69°$.

$Z(1)/Z_{min}=Exp\ [-0.10]\ sin\ [70.59]=0.853$, Eq. (11).

$Q_s(1)=Q_{sn} \times Z(1)/Z_{min}=5.65 \times 10^{21} \times 0.853= 4.82 \times 10^{21}$ J yr^{-1}, Eq. (15).

Average annual evaporation in tropics E=6.08 mm d^{-1}, data section.

Average annual evaporation in El Niño region E=6.08 mm d^{-1} x 365 d yr^{-1} x $A_n=6.08 \times 365 \times 4.91 \times 10^{13}=1.09 \times 10^{17}$ kg yr^{-1}.

Air mass flow rate in El Niño region $M=E/W_s=1.09 \times 10^{17}/0.0238=4.58 \times 10^{18}$ kg yr^{-1}, Eq. (17).

Oceanic Niño Index (ONI) for 1997$=2 \times Q_s(1) \times W_s/[E \times C_p]= 2 \times 4.82 \times 10^{21} \times 0.0238/(1.09 \times 10^{17} \times 1000)=2.11$°C, Eq. (18).

Similar calculations are conducted for the oscillation of the period of time between 1996 and 2014. For the oscillation that followed, residual energy is carried over. Also, an increase in global average sea surface temperature of nearly 0.073 °C per decade is assumed based on [24]. Results of the calculations are tabulated in Table 3, and a plot of the theoretically calculated Oceanic Niño Index is presented in Fig. 2.

Major contributors of calculation errors are A_n, Q_{sn}, and E. Based on [21] evaporation error is ±9%. The theoretical value of Q_{sn} has the same margin of error of evaporation because surface water evaporation is the basis for calculating poleward heat transport. The accuracy in estimating the area of El Niño region depends on surveying methodologies used, which could be reasonably accurate in the era of GPS and remote sensing. Therefore, the estimated calculation error of the theoretical Oceanic Niño Index could be within ±20%.

Discussion And Conclusions

The Oceanic Niño Index as defined and calculated by [4, 5] includes all sources of heat exchanged in El Niño region 3.4. Figure 1 illustrates graphically in blue color Index values for the months of November, December, and January. These are typical months when El Niño events occur. The graph in red color is the annual average value of the Index prepared by the

author. The theoretically calculated plot of Fig. 2 is produced by assuming that El Niño heat, Q_{sn}, and El Niño area, A_n, have constant values for the entire period of time in consideration between 1996 and 2020. A comparison between Fig. 1 and Fig. 2 may yield the conclusion that an overall agreement between the theoretically calculated and observed Oceanic Niño Indexes appears to exist. The graphs show damped oscillation with time as expected from an air hammer. At the beginning of a cycle, the plot of Fig. 2 closely resembles that of November, December, and January of Fig. 1. Thereafter, the plot approaches the annual average. Between 1996 and 2002, the amplitudes and phase angles of the theoretical oscillation fall well within the observed amplitudes. Between 2002 and 2009, the observed average values exhibit variability. Thereafter, the agreement resumes.

A temporary departure between the calculated and observed plots is expected. The reason is that the values of the observed Index include variability of all sources of heat exchange in El Niño region including but are not limited to typhoon count cycle, eleven-year solar cycle, global temperature rise, and the potential impact of volcanic eruptions. Conversely, the calculated index is relative to oscillation having its own thermodynamic parameters, triggered by initial conditions of air hammer. Seasonal or inter-annual climate variability may alter the measured Oceanic Niño Index but not the theoretically calculated index. This may explain the observed temporary departure between the indexes, and this understanding may be utilized in projecting Oceanic Niño Indexes.

However, a closer examination of the plots and Table 3 reveals that plot markers are not aligned. For time t=1 yr, phase angle is 70.37° instead of 90°, and the ratio $Z(t)/Z_{min}$ is equal to 0.852 instead of 1.0. These discrepancies may be practically eliminated by altering the values of El Niño heat, Q_{sn}, El Niño area, A_n, and air density in El Niño region, δ_n, within error margins. After all, their values used in the calculation have been estimated based on data available at this time. Plot markers may be aligned reasonably well, and considerably better agreement between the plots may be obtained. Therefore, improvement in Index calculation potentially exists.

The derived Eq. (11) is a sinusoidal function whose amplitude contains a decay factor. The positive amplitude, or El Niño episode, must necessarily be greater than the succeeding negative amplitude, or La Niña episode, at all times. They are thus asymmetric. Also, they decrease exponentially with time, they are nonlinear. The equation may, therefore, be considered to represent ENSO, and may be used for calculation and projection of ENSO climatology. For instance, air density in El Niño region fluctuates with El Niño Southern Oscillation. If sea temperature of the region experiences a warming episode, air density decreases and region’s barometric pressure decreases and vice versa. These variations in tropical air pressure may alter wind patterns in the western hemisphere in particular and global climates in general. So does the height of tropical tropopause, it fluctuates with ENSO as well. The authors of [15] observed a decrease in the height of tropical tropopause during El Niño episodes and an increase during La Niña episodes. The existence of these cycles of air potential energy is in good agreement with the theoretical work and the proposed concept of air hammer.

Finally, the oscillators of ENSO described in the literature are likely to be effects of El Niño air hammer. As effects, they may well be considered for calculating the Oceanic Niño Index; however, Index projection with time may be a challenge to achieve based on this work. This may explain success and failure of ENSO model simulations discussed in Introduction.

Symbols And Abbreviations

A_n	Surface area of El Niño event, m^2
β	Volumetric thermal expansion of sea water, $°C^{-1}$
C_p	Specific heat of air mixture, J kg^{-1} $°C^{-1}$
Cp_{sw}	Specific heat of sea water, J kg^{-1} $°C^{-1}$
Δ, d	A symbol that denotes small variation
ΔT_{sn}	Anomalies of sea temperature in El Niño region, which is equal to Oceanic symbol that denotes small variation
	Niño Index, ONI
d^{-1}	Per day
d_m	Average depth of ocean mixed layer, m
δ	Average air density of the lower atmosphere, kg m^{-3}
δ_n	Average air density in El Niño region, kg m^{-3}
δ_{sw}	Density of sea water, kg M^{-3}
E	Evaporation in El Niño region before and after El Niño event, kg yr^{-1}
E_n	Evaporation in El Niño region during El Niño event, kg s^{-1}
ENSO	El Niño Southern Oscillation
Exp (x)	Exponential function of natural logarithm base, equal to e^x
F_z	Component of the resultant of atmospheric force in Z direction, N.
F_b	Force of air buoyancy, N
Fc	Force of Coriolis, N
F_{zn}	Component of atmospheric force in Z direction during El Niño event, N
g	Gravity acceleration, m s^{-2}
m	Mass of air between sea level and tropical tropopause in El Niño region,
	Kg
M_n	Air mass flow rate in El Niño region during El Niño event, kg s^{-1}
M	Air mass flow rate in El Niño region before and after El Niño event, kg s^{-1}
N	Newton
ONI	Oceanic Niño Index, °C
P	Pressure of the atmosphere, kPa
PHT	Poleward heat transport, J yr^{-1}.

Q_a	Heat gained by an arbitrary air mass, J kg^{-1}
Q_s	Heat removed from the surface by an arbitrary air mass, J kg^{-1}
Q_{sn}	El Niño heat, J
$Q_s(t)$	Heat anomaly of sea water in El Niño region, J
s	Second
t	Time in seconds or year, or a period of time under consideration
τ	Earth's revolution time around the sun, 3.15 x 10^7 s
T_{sn}	Sea temperature in El Niño region, °C
U	Internal energy of arbitrary air parcel, J
V	Volume of air mass, m^3
v	Air vertical velocity in El Niño region, m s^{-1}
v_h	Air velocity horizontal component in El Niño region, m s^{-1}
v_n	Air vertical velocity in El Niño region during El Niño event, m s^{-1}
V_r	Relative velocity between air mass in El Niño region and surface, m s^{-1}
W	Work produced by an arbitrary air mass, J kg^{-1}
W_s	Air humidity at saturation, kg water per kg dry air
W_t	Air humidity at tropical tropopause, 0 kg water per kg dry air
ω	Angular velocity of the earth around its rotation axis, radians s^{-1}
yr	Year
Z	Vertical coordinate, height above sea level, m
Z_{min}	Initial amplitude of ENSO oscillation, m
Z_T	Height of tropical tropopause, m

Declarations

ACKNOWLEDGEMENTS

The Author acknowledges that this manuscript is entirely authentic and genuine and the entire work has been prepared by the Author. This manuscript is not currently being considered for publication by other journals. No data has been fabricated or manipulated. Furthermore, the author declares no conflicts of interest with respect to the research, authorship, and publication of this manuscript. This publication is funded by the Author.

AUTHOR CONTRIBUTIONS

The Author, Nabil Swedan, produced the entire work including text, figures, and tables.

COMPETING INTERESTS

The author declares no conflicts of interest with respect to the research, authorship, and publication of this manuscript.

DATA AVAILABILITY

Anomalies of sea surface temperature are available online at https://www.crudata.uea.ac-uk/cru/data/temperature/, Temperature, Temperature data (HadCRUT4, CRUTEM4) climate research, under tab “Data for downloading and file formats,” Hadsst3-SH and Hadsst3-NH, University of East Anglia, Climate Research Unit, Norwich, U. K.

https://www.crudata.uea.ac-uk/cru/data/temperature/. Observed Oceanic Nino index is available online at National Oceanic and Atmospheric Administration website, Climate Prediction Center-ONI-NOAA, Cold & Warm Episodes by Season,

https://www.origin.cpc.necp.noaa.gov/products/analysis_monitoring/ensostuff/ONI_v5.php

References

1. Caviedes, C.N. *El Niño in History Storming Through the Ages* (University Press of Florida, Gainesville, Florida, U.S.A., 2001).
2. Trenberth, K. E. & Hoar, T. J. The 1990-1995 El Niño Southern Oscillation event: Largest on record. Geophysical Research Letters **23** (1), 57–60; https://doi.org/10.1029/95GL03602 (1996).
3. Trenberth, K. E. et al. Evolution of El Niño–Southern Oscillation and global atmospheric surface temperatures. Journal of Geophysical Research **107**, no. d8; https://doi.org/10.1029/2000JD000298 (2002).
4. NOAA. Description of Changes to Ocean Niño Index, Climate Prediction Center-ONI-NOAA, Cold & Warm Episodes by Season, Centered 30-year base period, National Oceanic and Atmospheric Administration, Manchester, MA, U.S.A. https://www.origin.cpc.necp.noaa.gov/products/analysis_monitoring/ensostuff/ONI_v5.php. (Website accessed September, 2021).
5. NCAR. Climate Data (Nino 1+2, 3, 3.4, 4; ONI and TNI), National Center for Atmospheric Research, Boulder, CO, U.S.A.; https://climatedataguide.ucar.edu (Website accessed July, 2021).
6. Wang, C. et al. El Niño-Southern Oscillation (ENSO): A review In *Coral Reefs of the Eastern Pacific* (eds. Glymn, P., Manzello, D. & Enochs, I.) 85-106 (Springer Science Publisher, Dordrecht, 2016); doi: 10.1007/978-94-017-7499-4_4
7. Wang, C. A review of ENSO theories. National Science Review **5**, 813–825; doi: 10.1093/nsr/nwy104 (2018).
8. An, I. S. & Jin F. F. Nonlinearity and Asymmetry of ENSO. Journal of Climate **17**, 2, 2399–2412; https://doi.org/10.1175/1520-0442(2004)017<2399:NAAOE>2.0.CO;2 (2004).
9. Hayashi, M., Jin F. F. & Stuecker, M. F. Dynamics for El Niño-La Niña asymmetry constrains equatorial-Pacific warming pattern. *Nat Commun* **11**, 4230 (2020); doi:/10.1038/s41467-020-17983-y (2020).
10. Li, J. et al. Interdecadal modulation of El Niño amplitude during the past millennium. Nature Climate Change **1**, 114–118; https://doi.org/10.1038/nclimate1086 (2011).
11. Lin, K. H., Van Ness, H. C. & Abbott, M. M. Thermodynamics in *Perry’s Chemical Engineers Handbook, 6th edn* (eds. Crawford, H. B. & Eckes, B. E.) 4-52 to 4-59 (Mc Graw-Hill, New York, 1984).
12. Swedan, N. Parameterization of energy cycles between the hemispheres. *Science Progress* **103**: issue 2; https://doi.org/10.1177/0036850420922773 (2020).
13. Lau, K. M. & Yang, S. Tropical Meteorology & Climate Walker Circulation in *Encyclopedia of Atmospheric Physics*, 2nd edn. (eds. Pyle, G. R., North, J.& Zhang, F.) (Elsevier, Amsterdam, Netherland, 2015).
14. Sharp, B. & Sharp, D., 1995. *Water Hammer Practical Solutions*, 2nd edn. (Butterworth-Heimann, Oxford, 1995).

15. Jaramillo, A., Dominguez C., Raga G. & Quintanar A. I. The combined QBO and ENSO Influence on Tropical Cyclone Activity over the North Atlantic Ocean. Atmosphere 2021, **12**(12),1588; https://doi.org/10.3390/atmos12121588 (2021).
16. Srokosz, M. A. & Bryden, H. L. Observing the Atlantic Meridional Overturning Circulation yields a decade of inevitable surprises. *Science* **348**: no. 6241; doi: 10.1126/science.1255575 (2015).
17. CRU. Temperature, Temperature data (HadCRUT4, CRUTEM4) climate research, under tab “Data for downloading and file formats,” Hadsst3-SH and Hadsst3-NH, University of East Anglia, Climate Research Unit, Norwich, U. K.; https://www.crudata.uea.ac-uk/cru/data/temperature/ (Website accessed March, 2020).
18. Fleagle, R. G. & Businger, J. A. *An Introduction to Atmospheric Physics*, 2nd edn (eds. Van Mieghem, J. & Hales A. L.) 4-2, 151–176, 415 (Academic Press, New York, 1980).
19. Gruber, A. & Levizzani, V. Assessment of Global Precipitation Products, World Climate Research Program, Global Energy and Water Cycle, WCRP-128, WMO/TD-No. 1430 (World Meteorological Organization, Geneva, Switzerland, 2008).
20. Chanduvi-acña, F. A study of Evaporation and Evapotranspiration in Peru, All Graduate Thesis and Dissetations 1555.Utah State University; https://digitalcommons.usu.edu/etd/1555 (1969).
21. Swedan, N. H. Calculation of Open Water Evaporation as a Climate Parameter. Journal of Water Resource and Protection **10**, 762–779; https://doi.org/10.4236/jwarp.2018.108043 (2018).
22. Goldberg, N. Air Conditioning, Heating, and Ventilation in *Mark’s Standard Handbook for Mechanical Engineers*, 10th edn. (eds. Avallone, E. A. & Baumeisterm, T. III) 12–86 (McGraw-Hill, New York, 1996).
23. Caballero, R. *Physics of the Atmosphere* 2-1, 3-1, 6-1 (IOP Publishing Ltd, Bristol, U. K., 2014).
24. IPCC. Intergovernmental Panel On Climate Change (IPCC) Fifth Assessment Report (AR5), Climate Change, The Physical Science Basis (eds. Stocker T. F. et al.) 2.4.2 (Cambridge University Press, Cambridge, U.K., 2013).

Figures

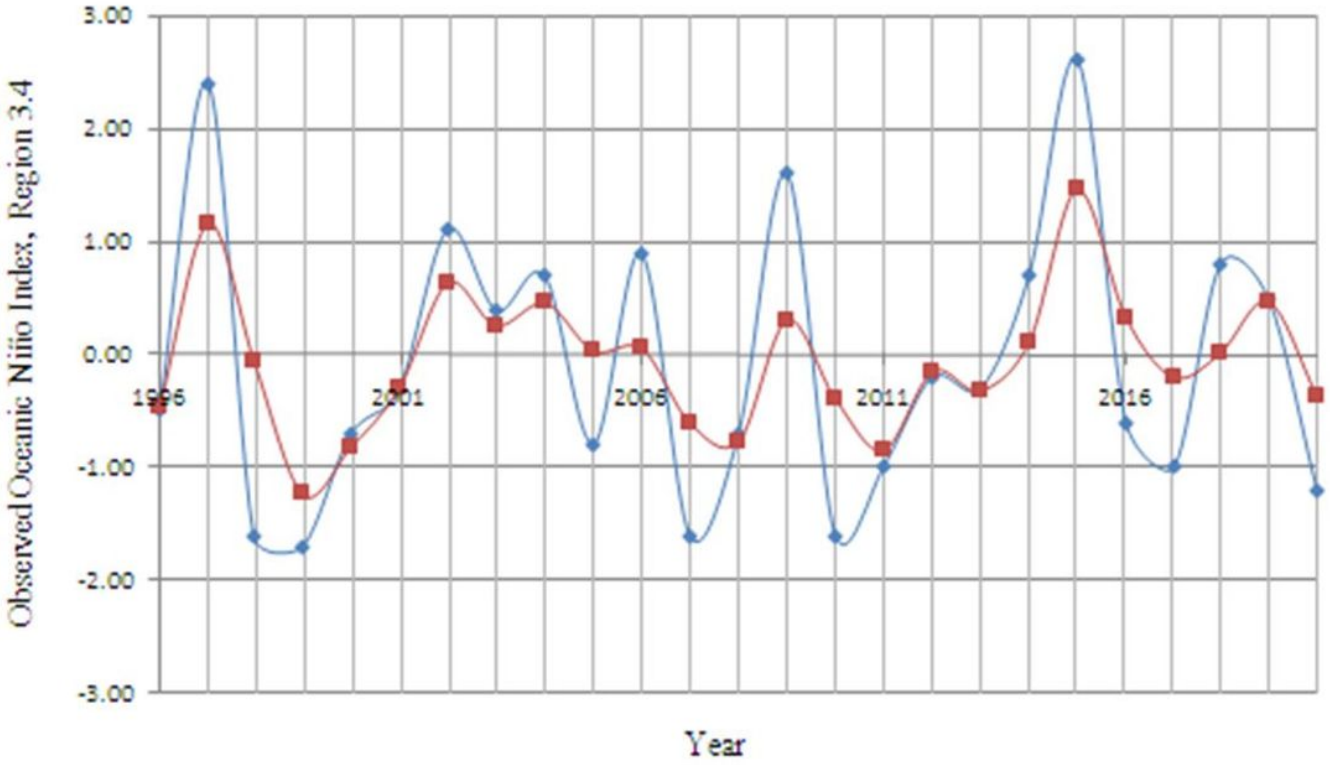

Figure 1

The observed Oceanic Niño Index for Niño region 3.4, °C. Annual average value of the Index is in red color and its average value for the months of November, December, and January is in blue color. These are the months of southern hemispheric summer in which El Niño typically occurs. The plots are obtained from last two columns of Table 1. Data source is National Oceanic and Atmospheric Administration [4].

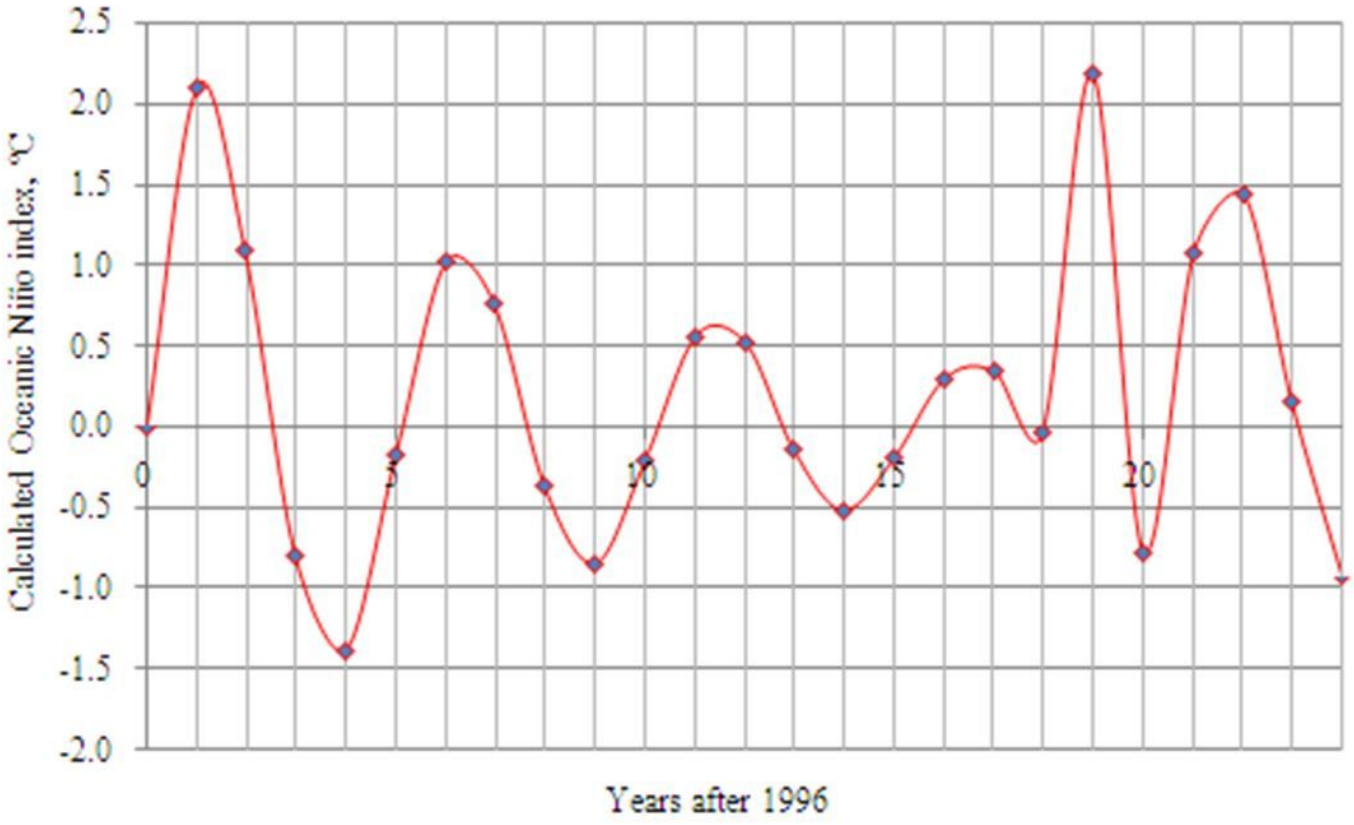

Figure 2

A plot of the calculated Oceanic Niño Index, obtained from Table 3, last row of the table.

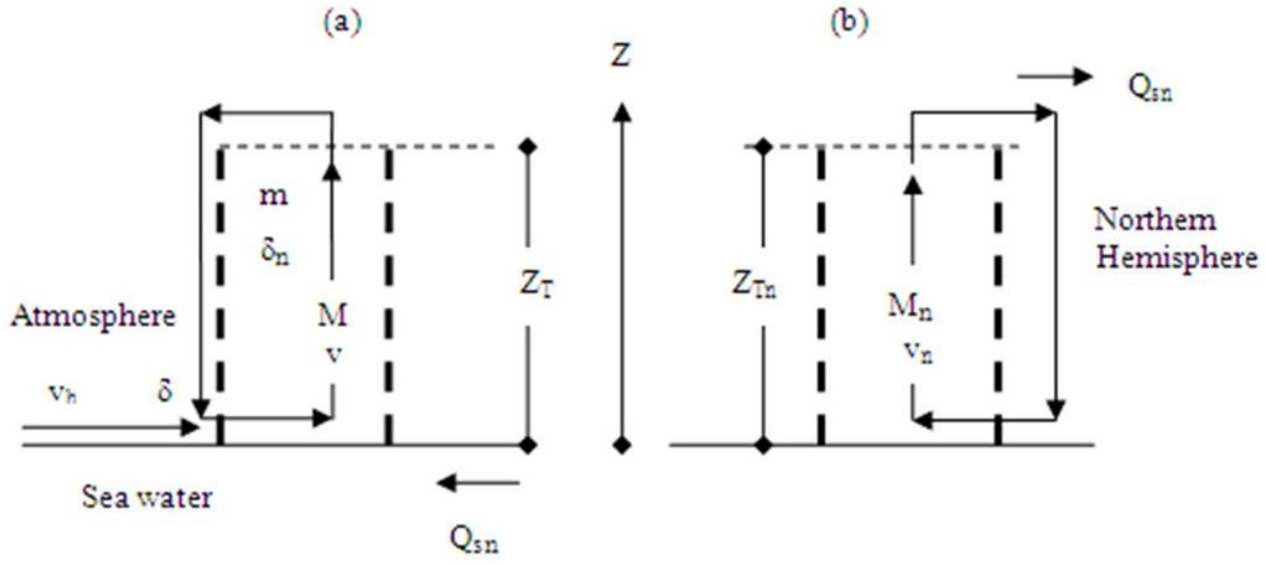

Figure 3

Heat transfer, air mass flow rate, and air volume of the lower atmosphere in El Niño region enclosed by the dashed lines. (a) Before and after El Niño event. (b) During El Niño event. M=Vertical component of the total tropical air flow rate before and after El Niño event, kg s^{-1}; v=Vertical velocity component of tropical winds in Z direction, m s^{-1}; v_h=Horizontal velocity component of tropical winds, m s^{-1}; Z_T=Height of tropical tropopause, m; Z_{Tn}=Height of tropical tropopause during El Niño event, m; Q_{sn}= Solar heat of El Niño, J; M_n=Vertical air mass flow rate during El Niño, kg s^{-1}; v_n=Vertical air velocity in Z direction during El Niño, m s^{-1}.